Properties of large scale ultra-high temperature ceramic matrix composites made by filament winding and spark plasma sintering

Highlights

- Toward Industrial manufacturing of ultra-high temperature ceramic matrix composites
- Full thermo-mechanical characterization and microstructure/properties correlation
- Superior elevated temperature properties than state-of-art materials

Graphical Abstract

Design

Manufacturing

Characterization

carbon fibres

UHTC slurry

Filament winding

Spark plasma sintering

UHTCMC tiles

tow

powders

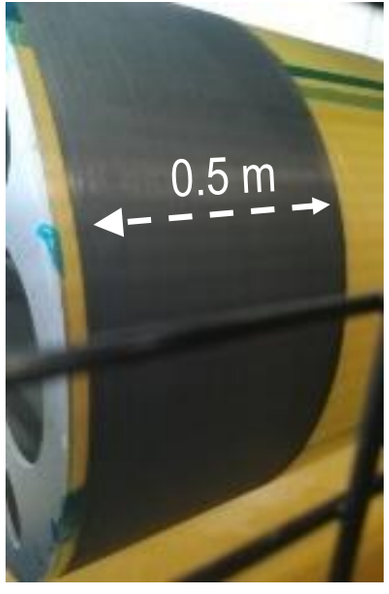

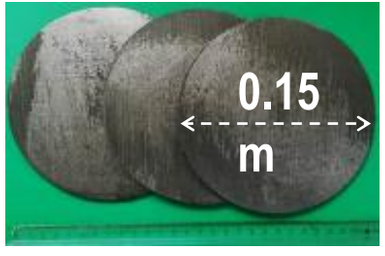

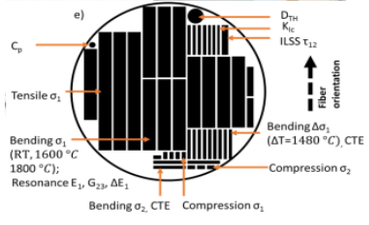

Physical properties			
Density	g/cm³	2.8±0.1	
Porosity via image analysis	vol%	18	
Open porosity via MIP	vol%	19	
Fibre amount	vol%	55	
Mechanical properties		**Longitudinal properties**	**Transverse properties**
Elastic modulus	GPa	135±6 (E)	14 (G)
Tensile strength, σ_t	MPa	312±18	-
Flexural strength, σ_f	MPa	631±12 650±24 (1600 °C) 676±21 (1800 °C)	25±1
Compression strength, σ_c	MPa	504±94	100±20
Interlaminar strength, ILSS	MPa	20.9±1.4	-
Fracture toughness, K_{Ic}	MPa·m$^{0.5}$	15.7±2.8	-
Coefficient of thermal expansion, α	10^{-6} °C^{-1}	1.8 (RT-1300 °C)	7.3
Apparent specific heat, C_p	J/(g·K)	-	0.7 2.0 (1500 °C)
Thermal diffusivity, D_{th}	mm²/s	-	6.0 3.5 (1500 °C) 4.4 (1950 °C)
Thermal conductivity, λ	W/(m·K)	-	10.9 19.5 (1500 °C)
Thermal shock resistance Retained flexural strength, $\Delta\sigma_f$	%	84 (ΔT_{th}=1500 °C)	-
Thermal shock resistance Retained modulus, ΔE	%	93 (ΔT_{th}=1500 °C)	-

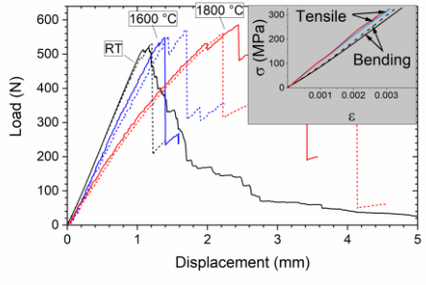

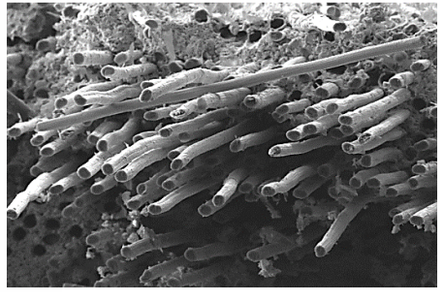

Properties of upscaled Ultra-High Temperature Ceramic Matrix Composites made by filament winding and spark plasma sintering

D. Sciti[1], P. Galizia[1], T. Reimer[2], A. Schoberth[3], C. Gutierrez-Gonzalez[4], L. Silvestroni[1], A. Vinci[1] L. Zoli[1],

[1] *National Research Council, Institute of Science and Technology for Ceramics, Via Granarolo 64, 48018 Faenza, Italy*

[2] *Institute of Structures and Design, German Aerospace Center, Pfaffenwaldring 38-40,70569, Stuttgart, Germany*

[3] *Airbus Defence and Space GmbH, 82024 Taufkirchen, Germany*

[4] *Nanoker Research S.L., Polígono de Olloniego, Parcela 22A - Nave 5, 33660 Oviedo, Principado de Asturias (Spain)*

ABSTRACT

In this paper, for the first time, we report the manufacturing and characterization of large UHTCMCs discs, made of a ZrB2/SiC matrix reinforced with PyC-coated PAN-based carbon fibres. This work was the result of a long term collaboration between different institutions and shows how it is possible to scale-up the production process of UHTCMCs for the fabrication of large components. 150 mm large discs were produced by filament winding and consolidated by spark plasma sintering and specimens were machined to test a large set of material properties at room and elevated temperature (up to 1800 °C). The extensive characterization revealed a new material with mechanical behaviour similar to CMCs, but with intrinsic higher thermal stability. Furthermore, the scale-up demonstrated in this work increases the appealing of UHTCMCs in sectors such as aerospace, where severe operating conditions limit the application of conventional materials.

Keywords: UHTCMC; Carbon fibres; mechanical properties; microstructure

1. Introduction

Ultra-high temperature ceramic matrix composites (UHTCMCs) are a new class of materials generated from integrating ultra-high temperature ceramic (UHTC) matrices with carbon or silicon carbide fibres [1]. The added value of these hybrid composites is the possibility to overcome the long standing problems of brittleness and low thermal shock resistance of UHTCs [2][3] on one

hand, and poor resistance to erosion/ablation at temperature >1600 °C of CMCs, on the other [4]. While the UHTCMCs are still at an infancy state, the state-of-the-art materials on which current technology is based, namely carbon fibre / silicon carbide (C_f/SiC) and silicon carbide fibre / silicon carbide (SiC_f/SiC) composites, are characterized by excellent intermediate temperature resistance, high thermal conductivity, low thermal expansion coefficient and good thermal shock resistance [5]. However, the poor oxidation resistance of this class of materials limits their applications below 1700 °C [6]. Therefore, the development of new ceramic matrix composites (CMCs) combining a mechanically robust and oxidation resistant matrix with a reinforcing phase, such as carbon fibres, could pave the way to a significant technological advance.

Several processing techniques have been adopted for the fabrication of UHTCMCs, most of which are re-adapted from the CMC technologies. The most investigated processes are [7][8]:

- Polymer Infiltration and Pyrolysis (PIP), where the UHTC phase is added to a SiC precursor [9][10];
- Reactive Melt Infiltration (RMI), where the carbon preforms are first impregnated with B-containing phases and then infiltrated with Zr-containing melts in special furnaces [11];
- Chemical Vapour Infiltration (CVI) with gaseous precursors of carbide phases, or with C precursors preceded by an infiltration stage with a UHTC containing slurry [12][13];
- Radio frequency - Chemical Vapour Infiltration (RF-CVI), a variant of conventional CVI where high values of matrix density are achieved in hours rather than weeks [14][15].

Authors of the present work have focused their studies on the processing of UHTCMCs, adopting the method of slurry impregnation and sintering. This method allowed to achieve high density composites, with high fractions of UHTC phase and a quite strong fibre/matrix interface [1][16][17]. The most investigated option for the matrix was ZrB_2, because it possesses the best combination of refractoriness (melting point 3250 °C), oxidation resistance and low specific weight (6.1 g/cm^3). Blends of ZrB_2 and SiC powders were studied to understand the effect of SiC addition on mechanical properties and oxidation resistance of UHTCMCs at intermediate (1650 °C) [18]. In other focused studies, the matrices were based on ZrC, TaC and HfC. The bending strength of these composites was measured up to 2100 °C [19][20], showing very promising results. As for the consolidation techniques, beside hot pressing, [1][16][17], it has been recently demonstrated that spark plasma sintering is an effective method to achieve densification in a few minutes for these composites, provided that the thermal cycle is finely calibrated to avoid excessive reactions at the interface with the fibre [21]. Finally, for the high temperature characterization, high enthalpy arc-jet tests demonstrated the capability of these composites to withstand temperatures as high as 2500 °C, with limited erosion [22][23][24].

In this work, we studied the filament winding technique to impregnate carbon fibres with ZrB_2 powders, using solvent-free water based slurries. Filament winding is an automated method for creating composite structures by winding filaments under tension over a rotating mandrel. This technique is frequently used in the aerospace field to manufacture carbon fibre reinforced phenolic resin products. To the best of our knowledge, it has been hardly used for manufacturing UHTCMCs [25]. The consolidation was carried out by spark plasma sintering. Both steps, impregnation and sintering, were carried out at industrial sites, namely Airbus DS for the filament winding and Nanoker Research for spark plasma sintering, in the perspective of material scale-up.

The produced discs were 150 mm in diameter allowing for an extended thermo-mechanical characterization, including bending and tensile testing, compression and interlaminar tests, as well as thermal shock resistance, fracture toughness, thermal expansion coefficient and thermal conductivity analysis. This extended characterization allowed for the first time to gain a more comprehensive overview of these new composites.

2. Experimental

Commercial ZrB_2 (Grade B, H.C. Starck, Germany, particle size range 0.5-6 µm, impurities (wt%): 0.2 C, 1.3 O, 0.19 N, 0.1 Fe, 1.4 Hf) and SiC powders (Grade UF-25, H.C. Starck, Germany, D50 0.45 µm) were used for the matrix preparation. PAN-derived carbon fibres (T800HB-6000, TORAYCA, Japan), diameter 5 µm, coated with a pyrolytic carbon (PyC), average thickness ~ 0.4 µm were supplied by AIRBUS (Airbus Defence and Space GmbH, 82024 Taufkirchen, Germany). The basic properties of these fibres are reported in Table 1.

Table 1: Properties of commercial T800HB-6000 fibre.

Fibre properties	
Tensile strength, MPa	5880
Tensile moduuls, GPa	294
Strain at failure, %	1.9
Density, g/cm^3	1.8
Filament diameter, µm	5
CTE, 10^{-6} °C^{-1}	-0.56
Specific heat, J/(g·°C)	0.75
Electrical resistivity, 10^{-3} Ω·cm	1.4
Thermal conductivity J/(cm·s·°C)	0.10
Chemical composition	C (>96%), Na+K <50 ppm

Water-based slurries containing a mixture of powders of ZrB_2 (as major ceramic phase) and SiC (as oxidation resistance aid) were prepared according to previously published procedure [17]. A filament winding equipment available at ARIANEGROUP was used to produce unidirectional fibre sheets impregnated with the slurry. Different parameters were tested to calibrate the ceramic/fibre volumetric ratio of the final material, with high, medium and low content of UHTC matrix, named **AIR-H**, **AIR-M** and **AIR-L** respectively and with fibre contents between 40-60 vol%. Then, impregnated layers of the three types of preforms were stacked in 0/0° sequence to get unidirectional fibre reinforced composites (UD samples) and to set the best fibre/matrix volumetric ratio. Afterwards, sheets with optimized ceramic/fibre volumetric ratio were selected to prepare discs with diameter Ø = 150 mm that were sintered by spark plasma sintering (SPS furnace HPD400, FCT Systeme GmbH, Germany) in a temperature range between 1700 and 1950 °C. The temperature was recorded through a pyrometer placed at the top of the machine and pointing at the centre of the blank (5 mm over the top surface). The bulk density of the sintered pellets was measured using Archimedes' method. The microstructures were analysed on polished and fractured surfaces using field emission scanning electron microscopy (FE-SEM, ΣIGMA, ZEISS NTS Gmbh, Germany). Local phase analysis of a selected composite was performed using a FEI Tecnai F20 ST TEM, with an acceleration voltage of 200 kV. The TEM was equipped with an EDAX EDS X-ray spectrometer PV9761 with a super ultra-thin window. The thin specimen was prepared by conventional cutting of a 3 mm diameter disk from the as-sintered material and mechanically grinding followed by ion beam thinning.

The fibre volumetric content and the residual porosity were measured by image analysis (Image-Pro Analyzer 7.0, v.7, Media Cybernetics, USA) on SEM micrographs of polished sections, to determine the final compositions. The open porosity was measured by mercury intrusion porosimetry (MIP) in the 0.0058-100 μm range (Pascal 140 and Pascal 240 series, Thermo Finnigan, U.S.A.).

Sintered discs were machined according to the sketch reported in Fig. 1. The following mechanical properties were measured onto unidirectional samples with 0/0° architecture:

-Young's modulus (E) and shear modulus (G) were determined using the resonance frequency method (ASTM E1875 – 08) on 60.0 mm × 10.0 mm × 2.5 mm bars (length, width, and thickness) using an H&P gain-phase analyzer (Tokyo, Japan) at RT. Six bars were tested.

-Tensile strength (σ_t) tests were conducted at room temperature at the German Aerospace Center (DLR, Stuttgart), on 100.0 mm × 10.0 mm × 2.5 mm bars (length, width and thickness) according to the EN 658-1:1999 norm.

- Compression strength (σ_c) was measured on pellets 6.0 mm × 3.0 mm × 3.0 mm (length by side lengths of the square cross-section) at room temperature using a universal Zwick-Roell testing machine (mod. Z050, Ulm-Einsingen, Germany) with crosshead speed 2 mm/min.

- Flexural strength (σ_f) was tested by 3-point bending at room temperature, 1600 °C and 1800 °C on 60.0 mm × 10 mm × 2.5 mm (length, width, and thickness) bars with a span-to-thickness ratio (s/t) of 20, according to EN 658-3:2002 standard. Room temperature tests were carried out in a Zwick-Roell testing machine at CNR, with crosshead speed 8 mm/min. High temperature tests at 1600 °C and 1800 °C were carried out in the INDUTHERM machine available at DLR with C_f/C-SiC CMC fixture for tests in argon flux. Three bars were tested for each temperature point. An estimation of strain to failure (ε) on stress-strain curves was carried out, according to the following equation:

$$\varepsilon = \frac{6Dt}{s^2} \quad (1)$$

Where D is the deflection at maximum force, t is the specimen thickness and s is outer support span.

- Interlaminar shear strength (ILSS) was evaluated by the short beam shear (SBS) test method. The 25.0 mm × 5.0 mm × 3.0 mm (length, width, and thickness) bars were fractured by 3-point bending tests at RT, according to EN 658-5:2003 standard using the above cited Zwick-Roell screw-driven load frame. A span of 15 mm (s/t = 5) and a crosshead speed 1 mm/min were used.

-Fracture toughness (K_{Ic}) was calculated by fracturing chevron notched beams (CNBs). The 25.0 mm × 2.0 mm × 2.5 mm (length, width, and thickness) CNBs were fractured according to EN 14425-3:2010 standard with a 4-point bending fixture with 10 - 20 mm spans in the Zwick-Roell testing machine. The chevron-notch tip depth and average side length were about 0.39 mm and 2.33 mm, respectively. Three specimens were loaded with a crosshead speed of 0.05 mm/min. The "slice model" equation of Munz et al. [26] was used to calculate K_{Ic}. The work-of-fracture (WoF) was calculated from fracture toughness tests as the area below the load-displacement curve divided by the double of the projected real surface (the un-notched area of the cross-section).

-For the thermal expansion coefficient (CTE), the relative dimensional change ($\Delta L/L_0$) vs temperature was recorded up to 1300 °C, with a heating rate of 10 °C/min, under flowing argon, using a Netzsch dilatometer (mod. DIL E 402, Netzsch Gerätebau, Germany), on 2 bars of 25.0 mm × 2.0 mm × 2.5 mm (length, width, and thickness). The linear CTE (α) was determined as the slope of the secant line joining the values at RT and 1300 °C.

-Thermal conductivity (λ) was obtained using the following equation:

$$\lambda(T) = \rho(T) \cdot C_p(T) \cdot D_{th}(T) \quad (2)$$

where λ is expressed in W/(m·K), ρ is the bulk density expressed in g/cm^3, C_p is the apparent specific heat in J/(g·K) and D_{th} is the thermal diffusivity in mm^2/s. D_{th} was measured up to 1950 °C under flowing Argon on a 10 mm diameter specimen with 2 mm height using a Netzsch laser flash diffusivity apparatus (mod. 427, Netzsch Gerätebau, Germany). C_p was measured up to 1500 °C using a Netzsch differential scanning calorimeter (mod. DSC 404 F1 Pegasus®, Netzsch Gerätebau, Germany).

-Thermal shock resistance was measured through the retained flexural strength ($\Delta\sigma_f$), after water-quenching from 1500 °C to 25 °C of bath temperature, by 4-point bending test on 25.0 mm × 2.5 mm × 2.0 mm^3 bars (length, width and thickness) with a lower span of 20 mm and an upper span of 10 mm was used (s/t = 5) in the same Zwick-Roell testing machine, 1 mm/min of crosshead speed. The strength after thermal shock was compared to the pristine strength tested on as sintered bars with same size. In analogy with strength we also measured the retained Young's modulus (ΔE), after water-quenching from 1500 °C to 25 °C of bath temperature, on 60.0 mm × 10.0 mm × 2.5 mm bars (length, width and thickness) at room temperature.

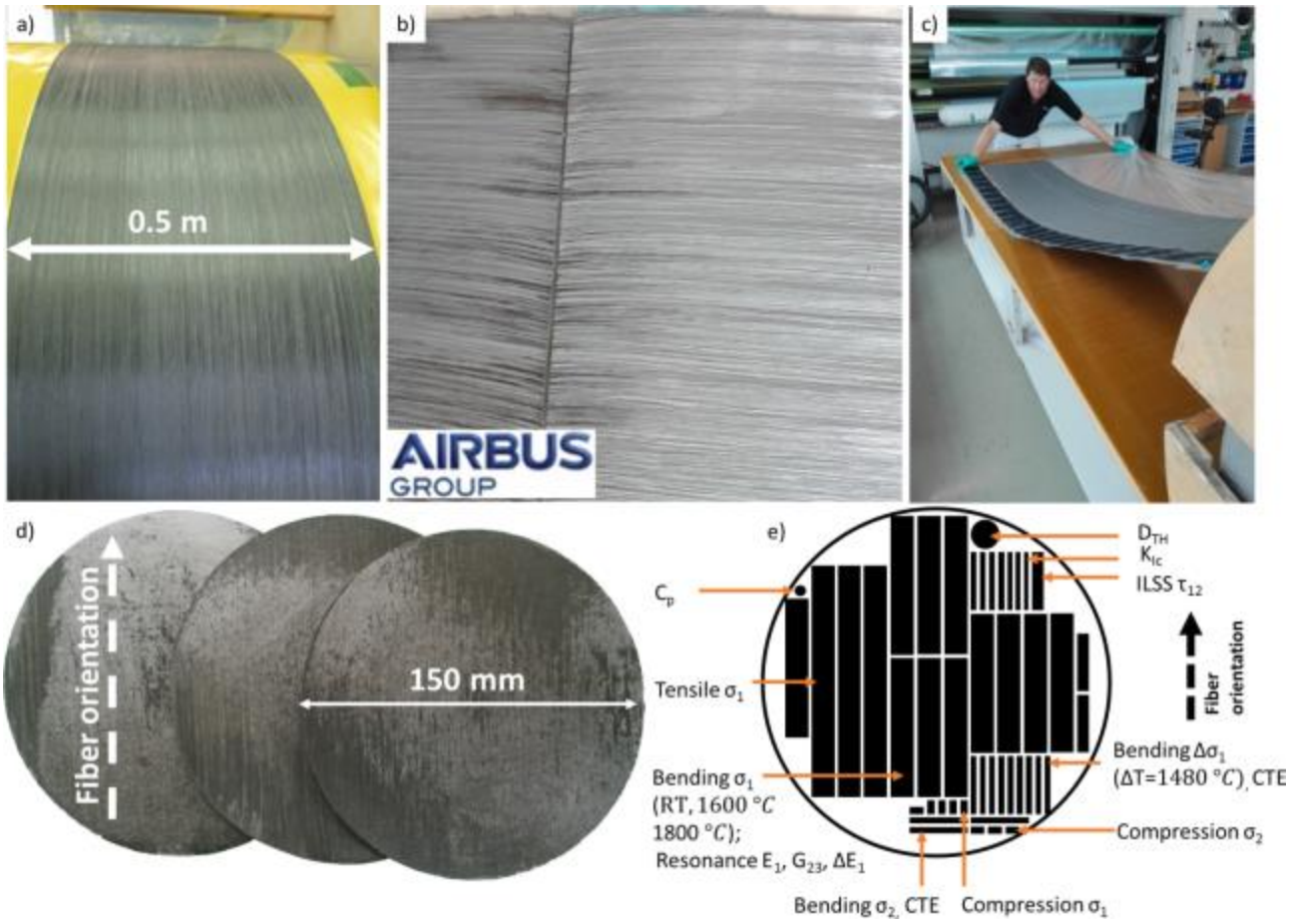

Fig. 1: a) Image of infiltrated filaments over a rotating mandrel with a diameter of 1 m and length of 0.5 m; b) detail of the infiltrated sheet after cutting necessary for subsequent unrolling, c) unrolled fibre sheet; d) 150 mm discs produced by overlapping fibre sheets and consolidation by SPS; e) the scheme of the specimens machining for mechanical characterization, achievable from a 150 mm large and 5 mm thick disc.

3. Results

3.1. Preliminary trials

Fig. 2a-c shows examples of microstructures obtained after preliminary trials to tune the fibre/matrix volumetric content ratio, with constant slurry concentration. The fibre filament can host a certain amount of slurry which depends on the specific characteristics of both powder particles and fibre, such as wettability and fibre surface area. Different settings were tried to calibrate the ceramic/fibre volumetric ratio and three compositions, labelled **AIR-L** (Fig. 2a), **AIR-M** (Fig. 2b) and **AIR-H** (Fig. 2c), were produced. Below a certain threshold, the slurry amount is too low to fill the voids between the fibres and wet all the available surfaces, which results in a composite with extremely high fibre volumetric content and too low matrix content (Fig. 2a). On the other hand, if the slurry content is too high compared to the available surface area, layers of unreinforced matrix regions appear between the infiltrated bundles (Fig. 2c). In every instance, dark spots are groups of fibres, stuck together because of the pyrolytic carbon coating (PyC). These agglomerated fibres were not penetrated by the slurry, irrespective of the infiltration set-up.

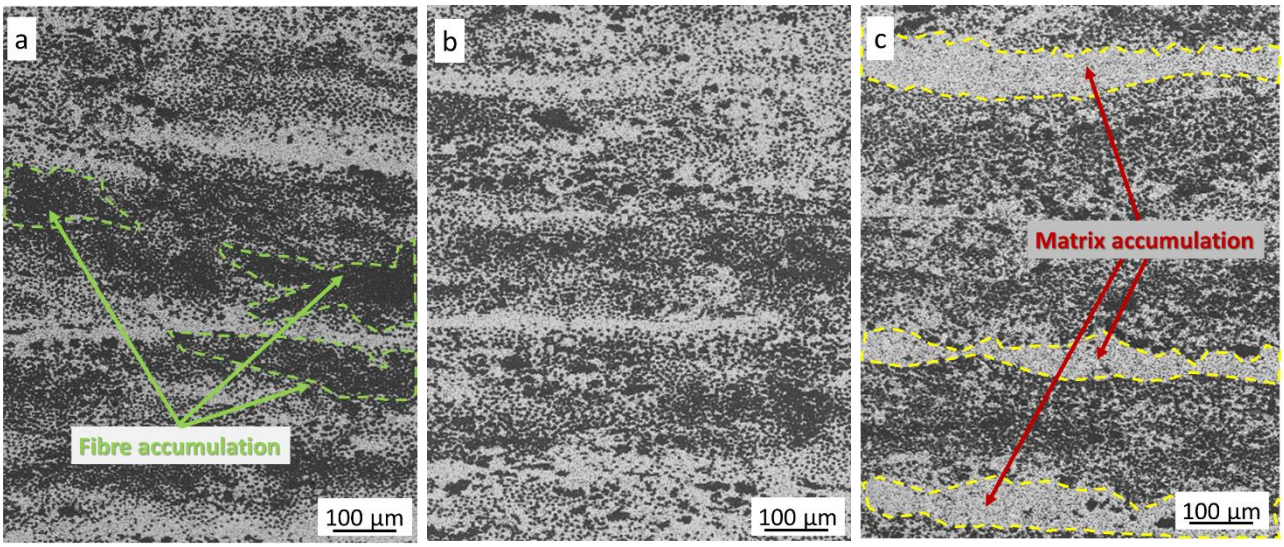

Fig. 2: Backscattered electron images of polished cross section of samples: a) AIR-L, b) AIR-M, c) AIR-H. Layers of unreinforced matrix are visible in sample AIR-H.

Densification through sintering at high temperature is the distinctive feature of these particular CMCs and the most critical aspect of the process because it impacts strength and environmental resistance. The most relevant microstructural features affecting environmental and mechanical performance are residual porosity and reactions at fibre/matrix interface. The matrix should be dense enough to ensure good oxidation/environmental resistance, but the interface with the fibre must be controlled to avoid fibre degradation and hence embrittlement.

Preliminary trials were carried out by spark plasma sintering to achieve a good matrix densification. High density could be achieved at optimized temperature values, whilst raising the temperature above 1900 °C, resulted in fibre degradation, despite the presence of the PyC coating. The tangible features of degraded fibres are loss of rounded shape, pronounced mechanical interlocking with the matrix due to grain penetration in the soft graphite, formation of reaction phases inside the coating or even inside fibre, as shown in previous works [21][27].

3.2 Microstructural features

Discs with diameter of 150 mm and thickness of 5 mm were manufactured using the best fibre/matrix volumetric ratio (**AIR-M**) for the impregnation step and applying an optimized densification cycle for the consolidation by spark plasma sintering. Typical microstructural features of a sintered disc are illustrated in Fig. 3. The experimental density measured by Archimedes' method was about 2.8 g/cm^3 (see Table 1), the fibre volumetric amount estimated by image analysis was around 55 vol%. According to the mercury intrusion porosimetry, the residual open porosity was 19%, with about 70 % of pore dimensions in the range 0.2 - 0.8 μm.

Polished sections in the directions perpendicular and parallel to the fibre axis are shown in Fig. 3. Fig. 3a evidences the fibre distribution in the matrix and the presence of porosities (visible as black holes) and its inset discloses a certain fibre disorder and misalignment even in the case of stacking parallel fibre sheets and the presence of vertical cracks due to coefficient of thermal expansion (CTE) mismatch between matrix and fibre [28]. The linear CTE of the matrix, from room temperature to 1300 °C, can be assumed to be similar to that of ZrB_2-SiC ceramics, e.g. ~7.5 × 10^{-6} °C^{-1} [29] while the CTE of the PAN-based carbon fibres according to the supplier is -0.4 ×10^{-6} °C^{-1}, in the axial direction. Therefore, a tensile residual stress would exist in the matrix and a compression residual stress would exist in the fibre in the axial direction of the fibre during cooling, respectively, that are responsible for the matrix micro-cracking perpendicular to the fibre axis direction. Extensive fibre pull-out, particularly detachment of the fibre from the PyC coating are appreciable in Fig. 3b.

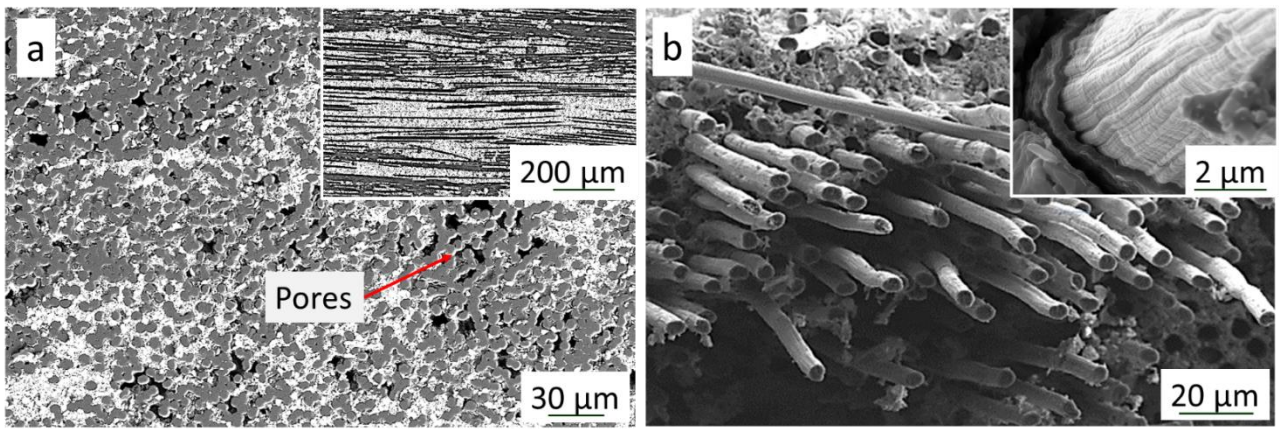

Fig. 3: a) Polished cross section of sample AIR-M, with fibre clusters and residual pores, inset in a) lateral view evidencing fibre misalignment b) Fibres pull-out in the fracture surface with magnification of the coating inner pull-out (inset).

Fig. 4a-d highlights details of the matrix/fibre interface. The coating thickness was not homogenous, ranging from 200-300 nm in some regions to 600-700 nm in other regions. Four different types of interfaces were recognized, two of which unreacted and two partially reacted. Fig. 4a shows fibre clusters that were not completely impregnated by the liquid slurry and thus formed weak fibre/fibre interfaces upon densification. Fig. 4b shows a region of the composite where fibres were partially infiltrated but the densification was not completed, leaving porosities and unreacted interfaces. Fig. 4c and Fig. 4d depict the situation of strong interfaces due to mechanical interlocking (c) and chemical reaction (d). Fig.4d shows a fibre with a thinner coating and tiny bright particles at the internal interface between coating and the fibre.

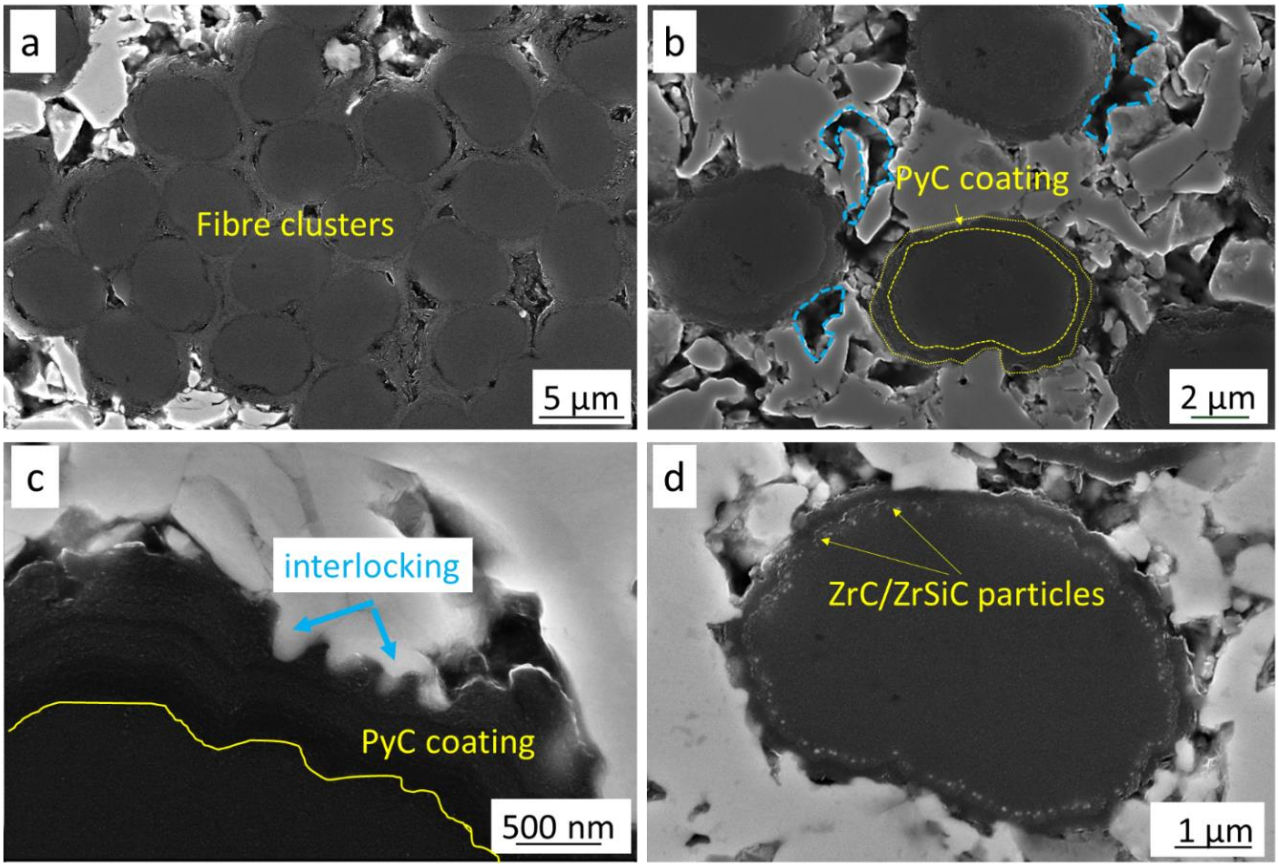

Fig. 4: a) fibre clusters highlighting fibre/fibre interfaces and detachment between fibre and coating. b) unreacted fibre/matrix interfaces in presence of porosities, dotted lines, c) a strong fibre/matrix interface due to mechanical interlocking of boride grains and carbon coating, d) reacted interfaces due to liquid phase penetration between fibre and coating.

Chemically reacted interfaces were further analysed by TEM (Fig. 5) which disclosed the reaction products formed at the matrix/coating interface.

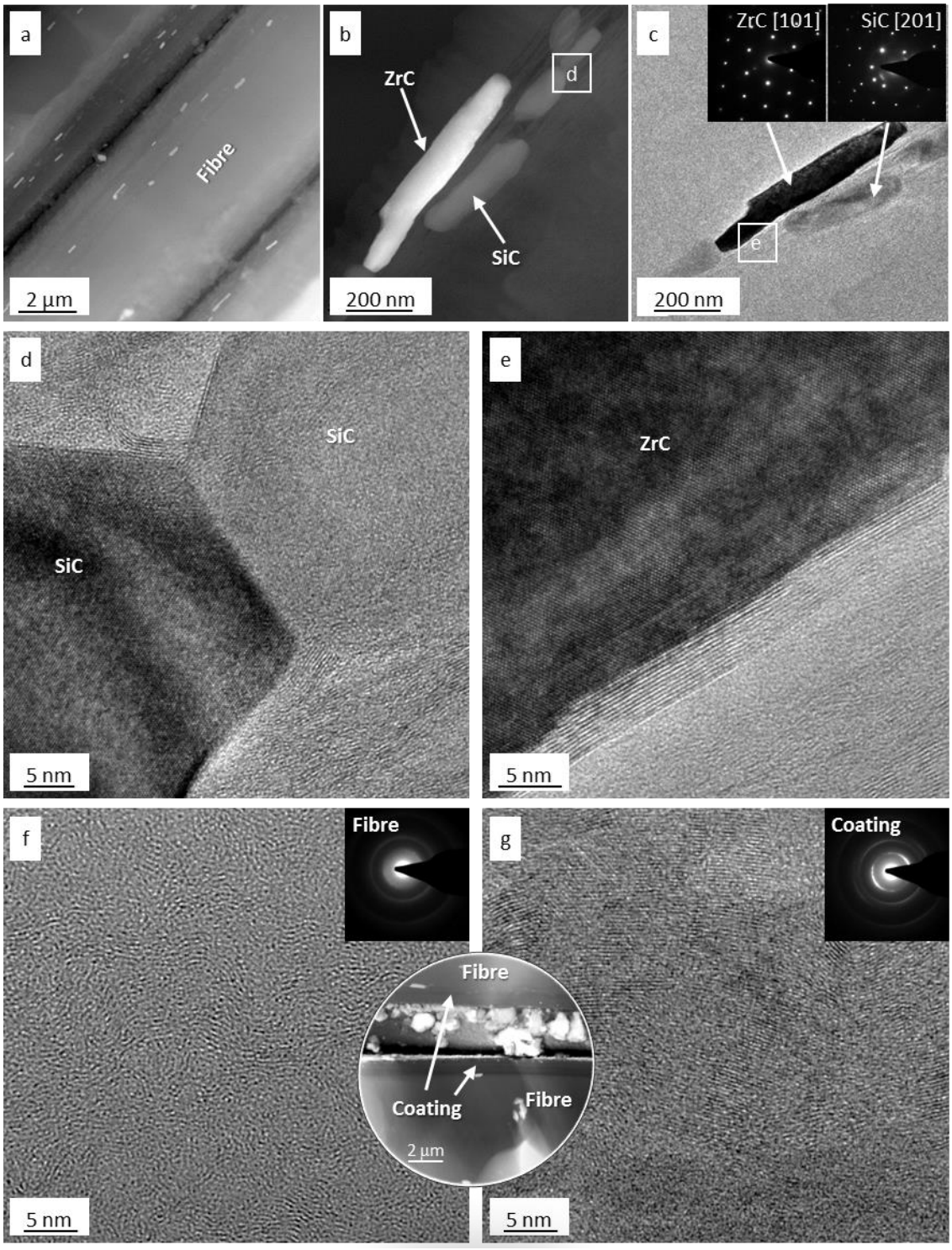

Fig. 5: TEM images showing a) the longitudinal fibre appearance covered with bright ZrC and SiC elongated particles magnified in the b) dark field and c) bright field magnified views with electron diffraction patterns inset. d) and e) are HR-TEM images showing coherent grow between the reaction particles and the partially crystalline PyC coating, whereas f) and g) show different crystallinity of the amorphous PAN-derived fibre and the PyC coating with low magnification image inset.

Similarly to previous investigations [30], reaction particles based on ZrC and SiC were ascertained, as evidenced by electron diffraction in Fig. 5a,b,c. Interestingly, these particles grown

along the fibre length longitudinally, following the pre-existing crystalline alignment of the PyC coating, as suggested by high resolution investigations in Fig. 5d,e. The disposition of such elongated bean-like particles possibly contributed to promote the fibre/coating inner pull-out upon fracture by acting as new class of critical flaws with periodic distribution. TEM analyses further revealed that the crystallinity degree of the carbon phases was higher for the PyC coating than for the fibres, that maintained a quite amorphous character, as indicated by the high resolution images and electron diffraction patterns compared in Fig. 5f,g. Comparison with pristine PAN-derived carbon fibre [31] confirmed that no internal microstructural changes, i.e. formation of turbostratic carbon ordered regions, occurred inside the carbon fibres upon densification at high temperature. Overall, most of the interfaces (90%) were akin to those depicted in Fig. 4a,b, therefore pull-out of fibres at fracture was very pronounced (Fig. 3b).

Microstructural analyses demonstrate that these composites contained microstructural defects, as it is typical of industrial products. These defects originated from imperfections in the starting fibres/preforms, such as variations in the coating thickness and presence of impenetrable fibre clusters. Other suspected sources of inhomogeneity could be due to the sintering treatment, because of temperature gradients between centre and edge of the large disc. However, extracting material samples from different positions of the disc, little variation of the features was found, therefore the sintering treatment of such large block of UHTCMC materials was considered to be quite homogeneous. It is likely that the thermal conductivity of these materials during heating was high enough to ensure a good homogenization of the temperature along the diameter, despite the relatively short dwell times.

3.3. Thermo-mechanical properties

All the thermo-mechanical properties of sample **AIR-M** are summarized in Table 2.

Table 2: Physical and mechanical properties of the UHTCMC composite

Physical properties			
Density	g/cm^3	2.8±0.1	
Porosity via image analysis	vol%	18	
Open porosity via MIP	vol%	19	
Fibre amount	vol%	55	
Mechanical properties		**Longitudinal properties**	**Transverse properties**
Elastic modulus	GPa	135±6 (E)	14 (G)

Tensile strength, σ_t	MPa	312±18	-
Flexural strength, σ_f	MPa	631±12	25±1
		650±24 (1600 °C)	
		676±21 (1800 °C)	
Compression strength, σ_c	MPa	504±94	100±20
Interlaminar strength, ILSS	MPa	20.9±1.4	-
Fracture toughness, K_{Ic}	$MPa \cdot m^{0.5}$	15.7±2.8	-
Coefficient of thermal expansion, α	10^{-6} °C^{-1}	1.8 (RT-1300 °C)	7.3
Apparent specific heat, C_p	J/(g·K)	-	0.7
			2.0 (1500 °C)
Thermal diffusivity, D_{th}	mm^2/s	-	6.0
			3.5 (1500 °C)
			4.4 (1950 °C)
Thermal conductivity, λ	W/(m·K)	-	10.9
			19.5 (1500 °C)
Thermal shock resistance			
Retained flexural strength, $\Delta\sigma_f$	%	84 (ΔT_c =1500 °C)	-
Thermal shock resistance			
Retained modulus, ΔE	%	93 (ΔT_c =1500 °C)	-

The Young's modulus of 135±6 GPa was measured from 6 bars extracted from different positions of the sample, showing a quite narrow dispersion. Since the modulus is strongly affected by microstructural features such as porosity and composition, the little scattering observed was considered as a good indicator of microstructural homogeneity, confirming the findings of microstructural analyses. This value was also in very good agreement with the value extracted from tensile testing, ~124 GPa (see below). The modulus of **AIR-M** is also in line with results on other uniaxial fibre reinforced UHTC materials. Indeed, it is significantly lower (135 vs 220 - 230 GPa) than that of UHTCMCs with higher modulus fibres and higher matrix density, consolidated either by PIP and or by hot pressing, [10][28], suggesting that fibre modulus and matrix porosity could be the dominant factors affecting this property in the composite.

The tensile tests, carried out for the first time on UHTCMCs of this type gave a value of 312±18 MPa. Typical stress strain curves are illustrated in Fig. 6, showing a linear behaviour until fracture. Analysis of the samples revealed that the crack pattern was quite complex and extended in longitudinal direction of the sample, along the fibres. Therefore, some influence of the clamping

cannot be ruled out. The optimization of tensile tests, in terms of specimen shape and deformation measurement, is still an open issue and, to the best of our knowledge, only few reliable data are available for the tensile strength of a UHTCMC reported in literature [8]. As previously mentioned, the recorded modulus was in good agreement with the average value determined by the resonance frequency method, ~124 GPa.

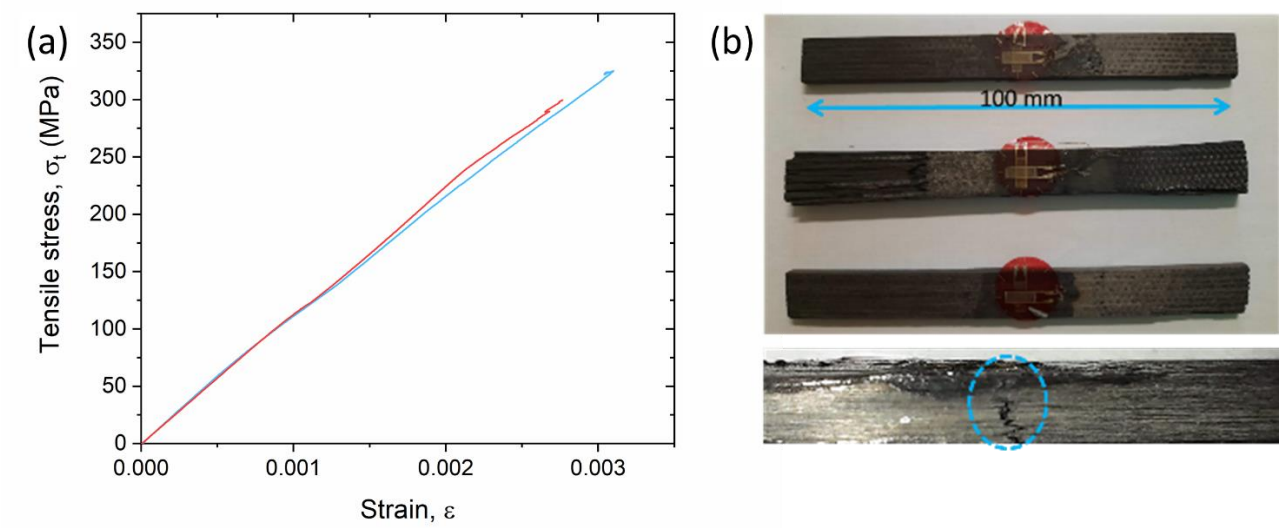

Fig. 6: a) Tensile stress/strain curves and b) images of the tested bars (top view) highlighting one example of crack propagation (side view).

The compressive strength (Fig. 7a) along the longitudinal direction was about 500 MPa and decreased by 5 times along the transverse direction, 100 MPa. The room temperature flexural strength achieved 631±12 MPa, showing a very narrow dispersion. The load displacement curves for bending tests at RT, 1600 °C and 1800 °C, Fig. 7b, featured a mixed mode of failure, with presence of interlaminar fracture as well [17][21][27]. Moreover, in the linear part, the slope was exactly overlapped with the tensile test curves (Fig. 7b inset). The strain to failure calculated according to Eq.(1) was 1.1 %.

Fig. 7c, shows the inside of the INDUTHERM chamber: the sample holder is placed inside a graphite die which is heated by an induction coil while Fig. 7d highlights a detail of a bar being tested under bending on the holder at 1600 °C. The interlaminar shear strength was 20 MPa, which is consistent with the microstructural features of the material that show high porosity, weak matrix-fibre interface, and 0/0° architecture. The load-displacement curves obtained at 1600 °C and 1800 °C (Fig. 7b) and the appearance of the tested specimens (Fig. 7e) suggests an increase of delamination with an increasing temperature.

As for elevated temperature properties, the flexural strength increased with increasing temperature from 630 MPa, to 650 MPa at 1600 °C and to 680 MPa at 1800 °C, respectively. This improvement, in agreement with the literature [1,28,32–34], was related to both increase of

mechanical properties of carbon fibres with temperature [35] and release of residual thermal stresses developed during the sintering process [28]. Likewise, as for the room temperature tests, all the load-displacement curves of bending tests at elevated temperature showed that the samples suffered from interlaminar shear, i.e. after reaching the maximum load, the stress drop was followed by a load increase.

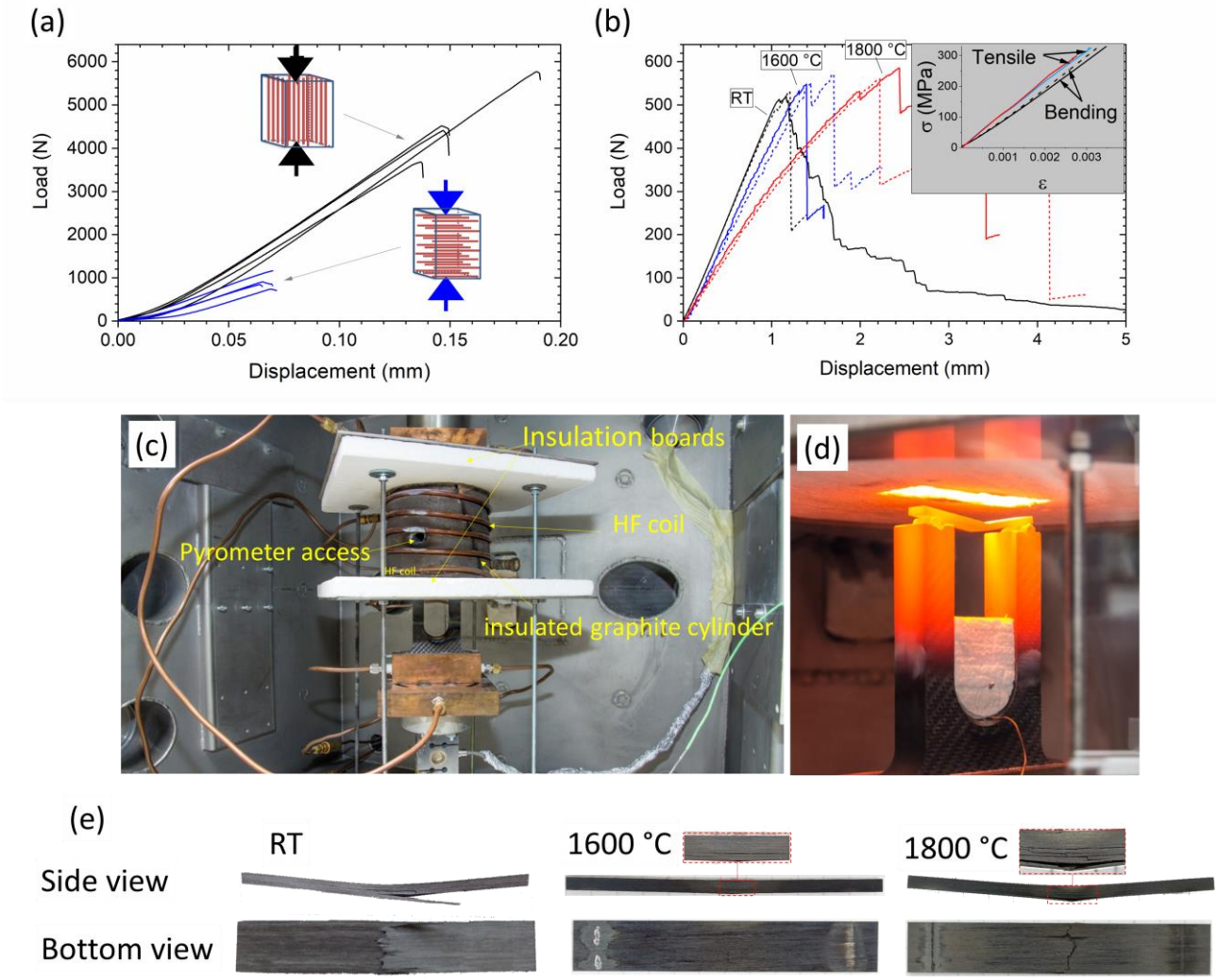

Fig. 7: Typical load-displacement curves obtained through a) compression tests along longitudinal and transverse direction and b) 3-point bending tests at RT, 1600 °C and 1800 °C. Inset in b) Stress-strain curves obtained through 3-point bending tests and tensile tests at RT. c) inside of the INDUTHERM facility chamber: the sample holder is placed inside a graphite die which is heated by an induction coil and d) detail of a sample being tested on the holder at 1600 °C inside INDUTHERM facility. e) side and bottom view of the specimens after bending test at RT, 1600 °C and 1800 °C.

The high strength and the graceful failure are well in agreement with the high toughness (15.7 MPa·$m^{0.5}$) and work-of-fracture (4.6 kJ/m^2) measured through CNB method. As shown in the

fracture surface of Fig. 3b, the PyC coating was effective in transferring the load from the matrix to the fibre, and the fracture occurred mostly between the coating and the fibre.

The linear CTE (α) between room temperature and 1300 °C was highly anisotropic, being 1.8×10^{-6} °C^{-1} along the longitudinal direction and 7.5×10^{-6} °C^{-1} along the transverse direction (Fig. 8a). The thermal conductivity along the transverse direction was almost constant at about 11 W/(m·K) from room temperature to 900 °C, due to simultaneous decrease of thermal diffusivity and increase of specific heat, then rapidly rose to about 20 W/(m·K) at 1500 °C (Fig. 8b), because of the stabilization of D_{th} and further increase of C_p. This range of thermal conductivity is low with respect to the 60 W/(m·K) typical of monolithic ZrB_2 [36]. The lower thermal conductivity should be ascribed to the low thermal conductivity of the fibre along the transverse direction and the large amount of pores and cracks within the matrix. On the other hand, a thermal conductivity of about 100 W/m/K is expected along the longitudinal direction owing to the superior conductivity of the fibre along their axis [37]. The thermal shock resistance (TSR) was hardly reported in the literature for composites materials; in this work we took inspiration from the procedure adopted for bulk ceramic materials. The retained strength after a sudden decrease from 1500 °C to RT was over 80% of the initial value (Fig. 8c) [38][39]. Using the same concept, the Young's modulus was also measured after quenching from 1500 °C, revealing an outstanding retention of 93% of the original value (see Table 2).

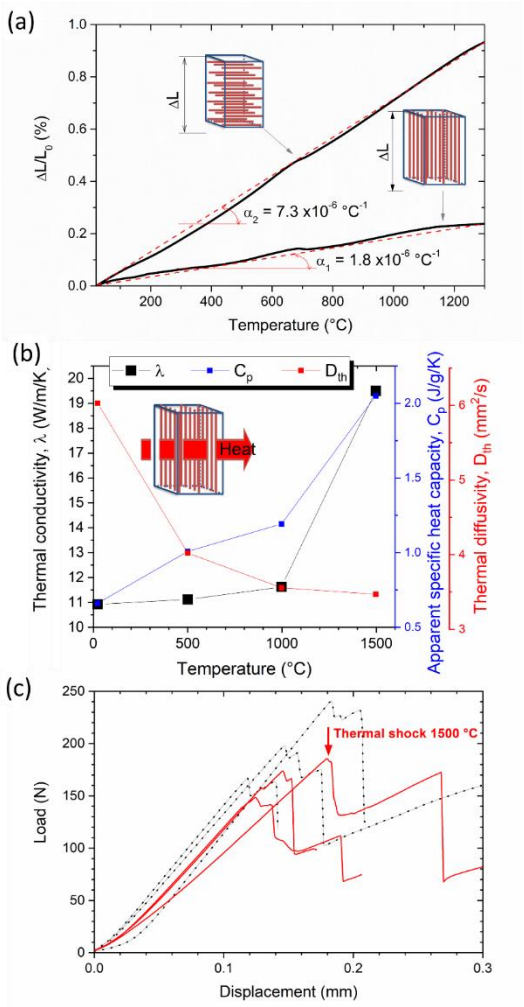

Fig. 8: Relative thermal expansions ($\Delta L/L_0$, solid lines) measured along transverse and longitudinal direction. The red dotted lines are the secant lines from which the linear coefficients of thermal expansion (α) were extrapolated. b) Thermal conductivity (λ), apparent specific heat capacity (C_p) and thermal diffusivity (D_{th}) vs. temperature. c) Typical load displacement curves obtained through 4-point bending tests before (dotted black curves) and after thermal shock (solid red curves).

4. Discussion

Overall, the excellent mechanical performance of this composite can be attributed to a good combination of microstructural features, including the high fibre volumetric content and the predominantly weak matrix fibre interfaces. The PyC coating was effective in protecting the fibres and even when partial reaction occurred, fibre inner debonding was possible by detachment between fibre and coating, therefore the load transfer mechanism occurred effectively, resulting in a damage tolerant composite.

As mentioned above, the matrix/fibre interface can change from completely unreacted to partially reacted. The formation of these different interfaces can be traced back to the densification mechanisms for these materials. The mechanisms active for these materials were mostly solid state ones, because the sources of liquid phases (e.g. Si-based or silica-based phases) were very limited in the starting compositions. At the interfaces, different behaviours were observed. When no matrix

powder could penetrate the bundle, weak fibre/fibre interfaces formed. In areas of limited slurry penetration, the physical distance between boride particles hindered the matrix densification and again the interfaces were not reacted and facilitated fibre pull-out. When more slurry penetrated the fibre bundles different sintering mechanisms could occur. Fibres are a source of carbon, that is a sintering additive for ZrB_2 [40]. Indeed, carbon or carbon-containing phases helped the removal of ZrO_2 from the boride particles via carbothermal reduction, making the surface more reactive and prone to densification. As a result, the densification was enhanced at the matrix/fibre interface, when enough powder was infiltrated between the fibres. Fig. 4c illustrates an example of a strong interface, characterized by mechanical interlocking of boride grains with the coating layers. When Si-O based phases were available, local densification proceeded by liquid phase sintering mechanisms. SiO-based liquid phases dissolved some zirconium, entered the loose layered structure of the PyC coating and were reduced to form ZrC and SiC species following the fibre alignment. In this case, fibre pull-out was permitted thanks to the inner fibre detachment from the coating. The sapient dosing of the processing parameters allowed therefore to achieve a good combination of matrix densification and weak interfaces.

As for the mechanical behaviour, a sound comparison with micromechanical models is still challenging. Use of formulas deriving from the lamination theory require the knowledge of the properties of the constituent phases. Some evident difficulties include the knowledge of how much the fibre properties were eventually altered by the sintering treatment. Another lack is the knowledge of the matrix properties that were affected by a large amount of porosity and cracks.

In spite of these limitations, some results can be further elaborated to speculate more on the properties. The Young's modulus of the 0/0° composite was 135±6 GPa by resonance method and 124±1 GPa through tensile tests. The modulus of fibre reinforced composites can be calculated with good approximation using the rule of mixture, starting from the moduli of the constituent phases and their volumetric content and assuming that Poisson ratio of matrix and fibre are not very different, as it is in most cases (0.15 for commercial T300 Toray fibres, [41], 0.12 for ZrB_2 [33]). The longitudinal carbon fibre modulus of T800HB is 294 GPa, as indicated by the supplier, while the modulus of a dense ZrB_2 matrix is ~500 GPa, as reported in [29]. With these values the resulting modulus of the composite should be around 390 GPa, e.g. much higher than the experimental value. Amongst the various affecting parameters, matrix porosity and cracking are considered the dominant factor mostly decreasing the matrix modulus [28][42]. These defects could drastically reduce the matrix modulus with respect to a reference pore-free value, down to 50-100 GPa [28]. Combining again the modulus of the porous matrix with fibre modulus, the calculated Young's modulus would result to be much closer to the experimental value (in the range 184-200 GPa for

matrix values around 50-100 GPa). Another factor contributing to the modulus reduction compared to a theoretical value could be the fibre misalignment that we observed experimentally. Even a misalignment of 5 degrees may lead to a decrease of 25 % of the Young's modulus [43].

It is still premature to discuss the strength properties in terms of the constituent phases properties. The tensile strength of the T800HB fibres, as given by the supplier, reaches almost 6 GPa, whilst the UHTCMC strengths (tensile, bending, compressive) are approximately 1/10 - 1/20 of the fibre tensile strength. Plenty of factors can explain this feature, including the actual strength distribution of fibre filament, the already cited fibre misalignment with respect to the loading direction, a possible carbon fibres loss of performance and damaging by crystallization of bean-like reaction products after densification and the matrix porosity that is known to decrease the composite properties [44]. As a matter of fact, both compressive strength and bending strength were higher than tensile strength and in this respect UHTCMCs behaved similar to other ceramic matrix composites [41][45]. For instance, in the work of Klatt et al [45], the bending strength of UD cross ply SiC/SiC composites was two times higher than tensile strength. Harris et al. [41] reported examples of CMCs where the bending strength was 1.5 - 2.5 times higher than tensile strength. Similar to CMCs, the compression strength of this UHTCMC was higher than its tensile strength, because the rigid ceramic matrix offered a greater level of support to the fibres, allowing their reinforcing potential to be realized, whereas the tensile strength was determined by features other than the fibre strength.

Thermal properties can be modelled using simple relations, starting from the constituent phases properties. For instance, the longitudinal and transverse CTE of a composite can be calculated as [46]:

$$\alpha_l = (E_f \cdot \alpha_f \cdot V_f + E_m \cdot \alpha_m \cdot V_m) / E_c \quad (3)$$

$$\alpha_2 = ((1 + \upsilon_m)\cdot\alpha_m\cdot V_m + (1+ \upsilon_f)\, \alpha_f \cdot V_f - \alpha_l (\upsilon_m \cdot V_m + \upsilon_f \cdot V_f) \quad (4)$$

where α_1 and α_2 are the longitudinal and transverse CTE, α_f and α_m, are the fibre and matrix CTEs. υ_m (0.12) and υ_f (0.15) are the Poisson moduli of matrix and fibres, respectively. Taking E_f = 294 GPa, $\alpha_f = -0.56 \times 10^{-6}$ °C^{-1} (as given by the supplier), V_f = 0.55, E_m=100 GPa, $\alpha_m = 7.5 \times 10^{-6}$ °C^{-1} [29], V_m=0.45, the value calculated from Eq. 2 is ~2 $\times 10^{-6}$ °C^{-1}, i.e. well in agreement with the experimental value and corroborating the assumed Young's modulus of the porous matrix (~100 GPa) used for calculation of the composite modulus. Considering that the transverse CTE of the fibres can be assumed to be around 6 $\times 10^{-6}$ °C^{-1} [47], the calculated composite CTE in the transverse direction with Eq. 2 is ~7 $\times 10^{-6}$ °C^{-1}, also in good agreement with the experimental value.

Thermal shock resistance of composites is another very challenging property to discuss. The thermal shock parameter, ΔTc, describing the maximum change in temperature that can occur without the initiation of cracks in an isotropic body, can be expressed in terms of strength (σ), Young's modulus (E), Poisson's ratio (v) and coefficient of thermal expansion (α).:

$$\Delta Tc = \sigma (1- v) / E\cdot \alpha \quad (5)$$

The calculation assumes an instantaneous change in surface temperature (infinite heat transfer) and is valid when the core of the body does not heat or cool prior to the surface reaching the temperature of the surrounding environment. Neglecting in first approximation the anisotropy of this composite and using experimental values of E (124 GPa), α_1 (1.8×10^{-6} $°C^{-1}$), tensile and bending strength as lower and upper bounds (310 - 630 MPa) for σ, and 0.13 as Poisson ratio of the composite, the maximum change in temperature that the composite can withstand is in the range 1220 - 2470 °C. This huge range needs refinement but is anyway consistent with the experimental results that indicate a 84 % of strength retention after the thermal drop of 1500 °C. In the present work it was not possible to raise temperature drops over 1500 °C because of experimental limitation in the maximum furnace temperature, however this rudimental calculation seems to suggest that these composites could withstand even greater thermal shocks, as required by the type of applications envisaged.

UHTCMCs are meant to replace C/SiC composites in applications that resist temperatures >1500 °C. There are some features in common between the two classes of materials, such as the need for a fibre coating because the matrix has a tendency to react with the fibres and the formation of transversal cracks due to CTE mismatch. C/SiC composites have excellent mechanical properties and oxidation resistance. These composites are generally produced by CVI or PIP or LSI (Liquid Silicon Infiltration) technologies, the choice depends on the application requirements. Very seldom CMCs were produced by hot pressing such as the UHTCMCs of the present work [48], moreover their properties are generally reported for complex preforms rather than for unidirectional reinforced composites. In spite of this, some comparative values can be found (see Table 3). The density of UHTCMCs composites is much higher than C/SiC due to the higher density of the ZrB_2 matrix, however, for the present case, the high fraction of porosity in the matrix maintained the density down to 2.8 g/cm^3. On one hand, porosity decreases weight and favours a weaker interface with the matrix, on the other it can be detrimental for the ablation/oxidation resistance [24] and for the strength, as previously illustrated. A direct comparison is still difficult because there are few

reported properties for UD 0/0° composites. see Table 3. The mechanical properties at room temperature of UHTCMCs are slightly inferior than PIP-C/SiC state-of-the-art materials with same fibre arrangement but lower porosity. One of the very few examples found in the literature of hot pressed C/SiC composites is reported in [49]. This composite with 55 vol% fibre content displayed a bending strength of 500 MPa and similar features in the load displacement curves with respect to UHTCMCs. Also the reported strain to failure was in agreement with that of the present UHTCMC [49], corroborating the similarities in mechanical behaviour between these two classes of composites. Sintered UHTCMCs are fast to produce and still possess a large margin of optimization (Table 3), besides having unrivalled properties at elevated temperature. Indeed, mechanical properties of CMCs at temperature higher than 1200 °C are rarely reported in literature, whilst UHTCMCs have shown a monotonic increase of flexural strength of UHTCMCs at least up to 1800 °C.

Table 3: Mechanical and thermo-physical properties of C/SiC composites reinforced with unidirectional fibre cloths compared with the present developed UHTCMC.

Property	PIP-C/SiC UD 0/0°	HP C/SiC UD 0/0°	UHTCMC
Reference	[50]	[49]	This work
Density (g/cm^3)	1.8	2.3	2.8
Porosity (vol%)	10	4.9	18
Fibre amount (vol%)	46	55	55
σ_t (MPa)	470	-	312
ε_t (%)	0.5	-	1.1
E (GPa)	145	-	124-135
σ_f (MPa)	-	500	631

5. Conclusions

For the first time, UHTCMC large discs with a diameter up to 150 mm of C/ZrB_2-SiC were produced through the optimized filament winding process and spark plasma sintering. A good densification of ZrB_2-based matrix was achieved while keeping a moderate interface reaction. Fibre/matrix volumetric ratio, matrix densification, and fibre/matrix interactions of UHTCMCs were tuned by different settings. The resulting composite had an intermediate density, 2.8 g/cm^3, high volumetric fibre fraction and 19 % of open porosity. Extensive microstructural and thermos-mechanical characterization revealed a promising material characterized by remarkable structural

properties such as tensile, compressive and flexural strength of 300, 500 and 630 MPa, respectively, and a fracture toughness of 16 MPa·$m^{0.5}$. All the properties measured at elevated temperature were higher than those at room temperature. Flexural strength monotonically increased up to 1800 °C. These structural properties coupled with the thermal shielding promised by the densified ZrB_2-based matrix and the facile scalability of the process push these composites among the desiderata materials list of aerospace designers.

The thermal shock resistance coupled with damage tolerance makes UHTCMCs very attractive also for reusable applications where neither C/SiC nor the C/C can be used.

Acknowledgements

This work received support by the European Union's Horizon 2020 research and innovation programme under Grant Agreement n° 685594. (C^3HARME: Next Generation Ceramic Composites for Harsh Combustion Environment and Space). Authors wish to acknowledge P. Mittermeier (AIRBUS), F. Meistring (ARIANEGROUP) for supplying coated PAN-based carbon fibres and for technical support during the filament winding procedure, S. Rivera (Nanoker Research S.L.) for SPS cycles and N. Gilli for technical support during TEM session.

Bibliography

[1] L. Zoli, A. Vinci, P. Galizia, C. Melandri, D. Sciti, On the thermal shock resistance and mechanical properties of novel unidirectional UHTCMCs for extreme environments, Sci. Rep. 8, (2018) Article number: 9148 https://doi.org/10.1038/s41598-018-27328-x.

[2] W.G. Fahrenholtz, G.E. Hilmas, I.G. Talmy, J.A. Zaykoski, Refractory diborides of zirconium and hafnium, J. Am. Ceram. Soc. 90 (2007) 1347–1364. doi:10.1111/j.1551-2916.2007.01583.x.

[3] E.P. Simonenko, N.P. Simonenko, V.G. Sevastyanov, N.T. Kuznetsov, ZrB_2/HfB_2–SiC Ceramics Modified by Refractory Carbides: An Overview, Russ. J. Inorg. Chem. 64 (2019) 1697–1725. doi:10.1134/S0036023619140079.

[4] N.P. Padture, Advanced structural ceramics in aerospace propulsion, Nat. Mater. 15 (2016) 804–809. doi:10.1038/nmat4687.

[5] W. Krenkel, Ceramic Matrix Composites: Fiber Reinforced Ceramics and their Applications, 2008. doi:10.1002/9783527622412.

[6] B. Mainzer, R. Jemmali, P. Watermeyer, K. Kelm, M. Frieß, D. Koch, Development of damage-tolerant ceramic matrix composites (SiC/ SiC) using Si-BN/SiC/pyC fiber coatings

and LSI processing, J. Ceram. Sci. Technol. 8 (2017) 113–120. doi:10.4416/JCST2016-00095.

[7] L.M. Rueschhoff, C.M. Carney, Z.D. Apostolov, M.K. Cinibulk, Processing of fiber-reinforced ultra- high temperature ceramic composites: A review, Int. J. Ceram. Eng. Sci. 2 (2020) 22–37. doi:10.1002/ces2.10033.

[8] V. Rubio, J. Binner, S. Cousinet, G. Le Page, T. Ackerman, A. Hussain, P. Brown, I. Dautremont, Materials characterisation and mechanical properties of Cf-UHTC powder composites, J. Eur. Ceram. Soc. 39 (2019) 813–824. doi:10.1016/j.jeurceramsoc.2018.12.043.

[9] Q. Li, S. Dong, Z. Wang, G. Shi, Fabrication and properties of 3-D Cf/ZrB2-ZrC-SiC composites via polymer infiltration and pyrolysis, Ceram. Int. 39 (2013) 5937–5941. doi:10.1016/j.ceramint.2012.11.074.

[10] F. Servadei, L. Zoli, P. Galizia, A. Vinci, D. Sciti, Development of UHTCMCs via water based ZrB2 powder slurry infiltration and polymer infiltration and pyrolysis, J. Eur. Ceram. Soc. 40 (2020) 5076-5084. doi:10.1016/j.jeurceramsoc.2020.05.054.

[11] M. Kütemeyer, T. Helmreich, S. Rosiwal, D. Koch, Influence of zirconium-based alloys on manufacturing and mechanical properties of ultra high temperature ceramic matrix composites, Adv. Appl. Ceram. 117 (2018) 62–69. doi:10.1080/17436753.2018.1509810.

[12] L. Li, Y. Wang, L. Cheng, L. Zhang, Preparation and properties of 2D C/SiC–ZrB_2–TaC composites, Ceram. Int. 37 (2011) 891–896. doi:https://doi.org/10.1016/j.ceramint.2010.10.033.

[13] S. Tang, J. Deng, S. Wang, W. Liu, K. Yang, Ablation behaviors of ultra-high temperature ceramic composites, Mater. Sci. Eng. A. 465 (2007) 1–7. doi:10.1016/j.msea.2007.02.040.

[14] V. Rubio, P. Ramanujam, J. Binner, Ultra-high temperature ceramic composite, Adv. Appl. Ceram. 117 (2018) 56–61. doi:10.1080/17436753.2018.1475140.

[15] A. Paul, S. Venugopal, J.G.P. Binner, B. Vaidhyanathan, A.C.J. Heaton, P.M. Brown, UHTC-carbon fibre composites: Preparation, oxyacetylene torch testing and characterisation, J. Eur. Ceram. Soc. 33 (2013) 423–432. doi:10.1016/j.jeurceramsoc.2012.08.018.

[16] D. Sciti, A. Natali Murri, V. Medri, L. Zoli, Continuous C fibre composites with a porous ZrB2 Matrix, Mater. Des. 85 (2015) 127-134. doi:10.1016/j.matdes.2015.06.136.

[17] L. Zoli, D. Sciti, Efficacy of a ZrB2–SiC matrix in protecting C fibres from oxidation in novel UHTCMC materials, Mater. Des. 113 (2017) 207–213. doi:10.1016/j.matdes.2016.09.104.

[18] A. Vinci, L. Zoli, D. Sciti, Influence of SiC content on the oxidation of carbon fibre

reinforced ZrB2/SiC composites at 1500 and 1650 °C in air, J. Eur. Ceram. Soc. 38 (2018) 3767–3776. doi:10.1016/j.jeurceramsoc.2018.04.064.

[19] A. Vinci, L. Zoli, D. Sciti, J. Watts, G.E. Hilmas, W.G. Fahrenholtz, Influence of fibre content on the strength of carbon fibre reinforced HfC/SiC composites up to 2100 °C, J. Eur. Ceram. Soc. 39 (2019) 3594-3603. doi:10.1016/j.jeurceramsoc.2019.04.049.

[20] A. Vinci, L. Zoli, D. Sciti, J. Watts, G.E. Hilmas, W.G. Fahrenholtz, Mechanical behaviour of carbon fibre reinforced TaC/SiC and ZrC/SiC composites up to 2100°C, J. Eur. Ceram. Soc. 39 (2019) 780–787. doi:10.1016/j.jeurceramsoc.2018.11.017.

[21] L. Zoli, A. Vinci, P. Galizia, C.F. Gutièrrez-Gonzalez, S. Rivera, D. Sciti, Is spark plasma sintering suitable for the densification of continuous carbon fibre - UHTCMCs?, J. Eur. Ceram. Soc. 40 (2020) 2597-2603. doi:10.1016/j.jeurceramsoc.2019.12.004.

[22] R. Savino, L. Criscuolo, G.D. Di Martino, S. Mungiguerra, Aero-thermo-chemical characterization of ultra-high-temperature ceramics for aerospace applications, J. Eur. Ceram. Soc. 38 (2018) 2937–2953. doi:10.1016/j.jeurceramsoc.2017.12.043.

[23] S. Mungiguerra, G.D. Di Martino, A. Cecere, R. Savino, L. Zoli, L. Silvestroni, D. Sciti, Ultra-high-temperature testing of sintered ZrB2-based ceramic composites in atmospheric re-entry environment, Int. J. Heat Mass Transf. 156 (2020) 119910. doi:https://doi.org/10.1016/j.ijheatmasstransfer.2020.119910.

[24] S. Mungiguerra, G.D. Di Martino, A. Cecere, R. Savino, L. Silvestroni, A. Vinci, L. Zoli, D. Sciti, Arc-jet wind tunnel characterization of ultra-high-temperature ceramic matrix composites, Corros. Sci. (2019). doi:https://doi.org/10.1016/j.corsci.2018.12.039.

[25] S.R. Levine, E.J. Opila, M.C. Halbig, J.D. Kiser, M. Singh, J.A. Salem, Evaluation of ultra-high temperature ceramics for aeropropulsion use, J. Eur. Ceram. Soc. 22 (2002) 2757–2767. doi:10.1016/S0955-2219(02)00140-1.

[26] D.G. Munz, J.L. Shannon, R.T. Bubsey, Fracture toughness calculation from maximum load in four point bend tests of chevron notch specimens, Int. J. Fract. 16 (1980) R137-R141. doi:10.1007/BF00013393.

[27] D. Sciti, L. Zoli, A. Vinci, L. Silvestroni, S. Mungiguerra, P. Galizia, Effect of PAN-based and pitch-based carbon fibres on microstructure and properties of continuous Cf/ZrB2-SiC UHTCMCs, J. Eur. Ceram. Soc. (2020) in press. doi:https://doi.org/10.1016/j.jeurceramsoc.2020.05.032.

[28] P. Galizia, L. Zoli, D. Sciti, Impact of residual stress on thermal damage accumulation, and Young's modulus of fiber-reinforced ultra-high temperature ceramics, Mater. Des. 160 (2018) 803–809. doi:10.1016/J.MATDES.2018.10.019.

[29] F. Monteverde, Beneficial effects of an ultra-fine α-SiC incorporation on the sinterability and mechanical properties of ZrB2, Appl. Phys. A Mater. Sci. Process. 82 (2006) 329–337. doi:10.1007/s00339-005-3327-9.

[30] L. Silvestroni, D. Dalle Fabbriche, C. Melandri, D. Sciti, Relationships between carbon fiber type and interfacial domain in ZrB2-based ceramics, J. Eur. Ceram. Soc. 36 (2016) 17–24. doi:10.1016/j.jeurceramsoc.2015.09.026.

[31] R. Schierholz, D. Kröger, H. Weinrich, M. Gehring, H. Tempel, H. Kungl, J. Mayer, R.-A. Eichel, The carbonization of polyacrylonitrile-derived electrospun carbon nanofibers studied by in situ transmission electron microscopy, RSC Adv. 9 (2019) 6267–6277. doi:10.1039/C8RA10491C.

[32] J. Sha, S. Wang, J. Dai, Y. Zu, W. Li, R. Sha, High-temperature Mechanical Properties and Their Influence Mechanisms of ZrC-Modified C-SiC Ceramic Matrix Composites up to 1600 °C, Materials (Basel). 13 (2020) 1581. doi:10.3390/ma13071581.

[33] T. Cheng, X. Wang, R. Zhang, Y. Pei, S. Ai, R. He, D. Fang, Y. Yang, Tensile properties of two-dimensional carbon fiber reinforced silicon carbide composites at temperatures up to 2300 °C, J. Eur. Ceram. Soc. 40 (2020) 630–635. doi:10.1016/j.jeurceramsoc.2019.10.030.

[34] Y. Zhang, L. Zhang, L. Cheng, Y. Xu, Tensile behavior and microstructural evolution of a carbon/silicon carbide composite in simulated re-entry environments, Mater. Sci. Eng. A. 473 (2008) 111–118. doi:10.1016/j.msea.2007.05.015.

[35] C. Sauder, J. Lamon, R. Pailler, The tensile behavior of carbon fibers at high temperatures up to 2400 °C, Carbon 42 (2004) 715–725. doi:10.1016/j.carbon.2003.11.020.

[36] B.R. Golla, A. Mukhopadhyay, B. Basu, S.K. Thimmappa, Review on ultra-high temperature boride ceramics, Prog. Mater. Sci. 111 (2020) 100651. doi:10.1016/j.pmatsci.2020.100651.

[37] N.L. Hancox, R.M. Mayer, N.L. Hancox, R.M. Mayer, Thermal and Electrical Properties, in: Des. Data Reinf. Plast., Springer Netherlands, 1994: pp. 153–169. doi:10.1007/978-94-011-0707-5_7.

[38] W.R. BUESSEM, Thermal Shock Testing, J. Am. Ceram. Soc. 38 (1955) 15–17. doi:10.1111/j.1151-2916.1955.tb14546.x.

[39] C. Kastritseas, P.A. Smith, J.A. Yeomans, Thermal shock fracture in unidirectional fibre-reinforced ceramic-matrix composites, Compos. Sci. Technol. 65 (2005) 1880–1890. doi:10.1016/j.compscitech.2005.04.004.

[40] W.G. Fahrenholtz, G.E. Hilmas, S.C. Zhang, S. Zhu, Pressureless sintering of zirconium diboride: Particle size and additive effects, J. Am. Ceram. Soc. 91 (2008) 1398–1404. doi:10.1111/j.1551-2916.2007.02169.x.

[41] B. Harris, Engineering composite materials, London, 1999. doi:10.1016/0010-4361(87)90420-4.

[42] O. Yeheskel, O. Tevet, A New Assessment Method for the Bulk Modulus and the Poisson's Ratio of Porous Ceramics, J. Test. Eval. 28, (2000) 189-198. doi:10.1520/jte12094j.

[43] Y. Li, B. Stier, B. Bednarcyk, J.-W. Simon, S. Reese, The effect of fiber misalignment on the homogenized properties of unidirectional fiber reinforced composites, Mech. Mater. 92 (2016) 261–274. doi:https://doi.org/10.1016/j.mechmat.2015.10.002.

[44] K. Schönfeld, H. Klemm, Interaction of fiber matrix bonding in SiC/SiC ceramic matrix composites, J. Eur. Ceram. Soc. 39 (2019) 3557–3565. doi:https://doi.org/10.1016/j.jeurceramsoc.2019.05.025.

[45] E. Klatt, A. Frass, M. Frieß, D. Koch, H. Voggenreiter, Mechanical and Microstructural Characterisation of SiC- and SiBNC-Fibre Reinforced CMCs Manufactured via PIP Method Before and After Exposure to Air, J. Eur. Ceram. Soc. 32 (2012) 3861–3874. doi:10.1016/j.jeurceramsoc.2012.05.028.

[46] R.A. Schapery, Thermal Expansion Coefficients of Composite Materials Based on Energy Principles, J. Compos. Mater. 2 (1968) 380–404. doi:10.1177/002199836800200308.

[47] R. Kulkarni, O. Ochoa, Transverse and Longitudinal CTE Measurements of Carbon Fibers and Their Impact on Interfacial Residual Stresses in Composites, J. Compos. Mater. - J Compos MATER. 40 (2006) 733–754. doi:10.1177/0021998305055545.

[48] P. Galizia, D. Sciti, F. Saraga, L. Zoli, Off-axis damage tolerance of fiber-reinforced composites for aerospace systems, J. Eur. Ceram. Soc. 40 (2020) 2691–2698. doi:10.1016/j.jeurceramsoc.2019.12.038.

[49] Y. Ding, S. Dong, Q. Zhou, Z. Huang, D. Jiang, Preparation of C/SiC Composites by Hot Pressing, Using Different C Fiber Content as Reinforcement, J. Am. Ceram. Soc. 89 (2006) 1447–1449. doi:10.1111/j.1551-2916.2005.00872.x.

[50] W. Schäfer, W.D. Vogel, Faserverstärkte Keramiken hergestellt durch Polymerinfiltration, in: Keramische Verbundwerkstoffe, Wiley-VCH Verlag GmbH & Co. KGaA, Weinheim, FRG, 2006: pp. 76–94. doi:10.1002/3527607315.ch4.